JOURNAL OF APPLIED ELECTROCHEMISTRY 9 (1979) 615–621

Diffusion controlled inhibition of electrodeposition: impedance measurements

J. BRESSAN, R. WIART

Groupe de Recherche no. 4 du CNRS 'Physique des Liquides et Electrochimie', associé à l'Université Pierre et Marie Curie, 4 place Jussieu, 75 230 Paris Cedex 05, France

Received 19 October 1978

At low rotation speeds of a rotating disc electrode the diffusion-controlled inhibition of zinc deposition by lead acetate or tetrabutylammonium bromide emphasizes the existence of multiple steady states. With both zinc and nickel deposition, low frequency impedance measurements reveal an additional inductive loop associated with a diffusion-controlled inhibition of electrodeposition. From the relaxation time constant it has been concluded that this loop arises from a coupling between the inhibitor diffusion and interfacial processes slower than diffusion and involving, at least for zinc deposition, the slow renewal of active growth sites.

1. Introduction

It is known that the additives which modify the structure and properties of electrodeposits are generally inhibitors of the electrocrystallization process. In the electrode kinetics this inhibiting effect appears not only as a decrease in the overall rate of electrodeposition but also as specific changes in the rates of the various interfacial reactions leading to deposits. Such a situation has been observed particularly with butyne-2-diol 1,4 (B_2D_{14}) for nickel electrodeposition [1] and with lead acetate ($PbAc_2$) or tetrabutylammonium bromide (NBu_4Br) for zinc electrodeposition [2, 3].

Generally the additive molecules are consumed at the electrode and their concentration in the electrolyte is low, so that in practice their consumption rate is often controlled by convection and diffusion [4]. Under such conditions, the number of adsorbed molecules and consequently the inhibiting effect of these molecules on the rates of interfacial reactions are also controlled by mass transport [5]. Realizing such hydrodynamic conditions by using a rotating disc electrode, we measured the electrode impedance. The purpose of this paper is to present the experimental results for the inhibition of nickel electrodeposition by B_2D_{14} and of zinc electrodeposition by $PbAc_2$ and NBu_4Br.

2. Experimental

The electrolytic cell has been described previously [2]. A rotating disc electrode whose speed could vary between 0 and 5000 rev min^{-1} was used in order to prepare electrodeposits in well controlled hydrodynamic conditions. For nickel electrodeposition, the substrate was a brass cylinder and the anode was made of nickel supplied by Johnson Matthey (impurities < 30 ppm). The electrolytes investigated were as below.

2.1. *For zinc electrocrystallization*

The Leclanché cell electrolyte was as follows: 2·67 M NH_4Cl, x M $ZnCl_2$ (x = 0·48 and 0·72); pH adjusted to 5·2 with NH_4OH (density 0·92). The alkaline electrolyte used in the accumulators was as follows: 7 M KOH, 0·5 M ZnO.

The electrolysis temperature was 26 ± 0·2° C. These electrolytes were prepared with Merck (pro analysi) products. The additives were $PbAc_2$ (Merck pro analysi) and NBu_4Br (Fluka high purity).

2.2. *For nickel electrocrystallization*

The Watts electrolyte was as follows: 1·07 M $NiSO_4 \cdot 7H_2O$, 0·15 M $NiCl_2 \cdot 6H_2O$, 0·65 M H_3BO_3; pH adjusted with NH_4OH or H_2SO_4 (density

0021–891X/79/050615–07 $02·70/0

1·84). The electrolysis temperature was 50 ± 0·2° C. The Watts electrolyte was prepared with Prolabo products. The additive was B_2D_{14} (BASF purified by a bidistillation under low pressure).

Current–potential data and impedance measurements were made galvanostatically as described previously [2]. The ohmic drop was measured using an interrupter method [6, 7] and analogically compensated [8].

3. Results and discussion

3.1. *Nickel electrocrystallization*

For the additive-free Watts electrolyte, the current–potential curve plotted for a rotation speed, Ω, of 2000 rev min^{-1} is shown in Fig. 1a (curve 1). In the presence of 8 × 10^{-3} M B_2D_{14}, curve 5 is obtained for the same rotation speed. This speed is sufficiently high to produce a current–potential curve independent of mass transport so that the inhibiting effect of B_2D_{14} is not diffusion-controlled.

A typical impedance diagram obtained in the inhibitor-free electrolyte for currents higher than 1 mA is shown on Fig. 1b (obtained at point A on Fig. 1a). In the presence of 8 × 10^{-3} M B_2D_{14}, Fig. 1d (obtained at point C on Fig. 1a) is observed at the same current. A comparison of Figs. 1b and 1d shows that B_2D_{14} increases the transfer resistance and modifies the shape of the inductive loop, in agreement with previously reported results [1]. At the lowest frequencies (10^{-3}–0·3 Hz) an additional capacitive loop, which has not been mentioned until now, is observed.

For lower rotation speeds the inhibiting effect of B_2D_{14} becomes diffusion-controlled. Fig. 1a shows that the shift of polarization towards cathodic potentials decreases with rotation speed (curves 2, 3 and 4). Furthermore at a given

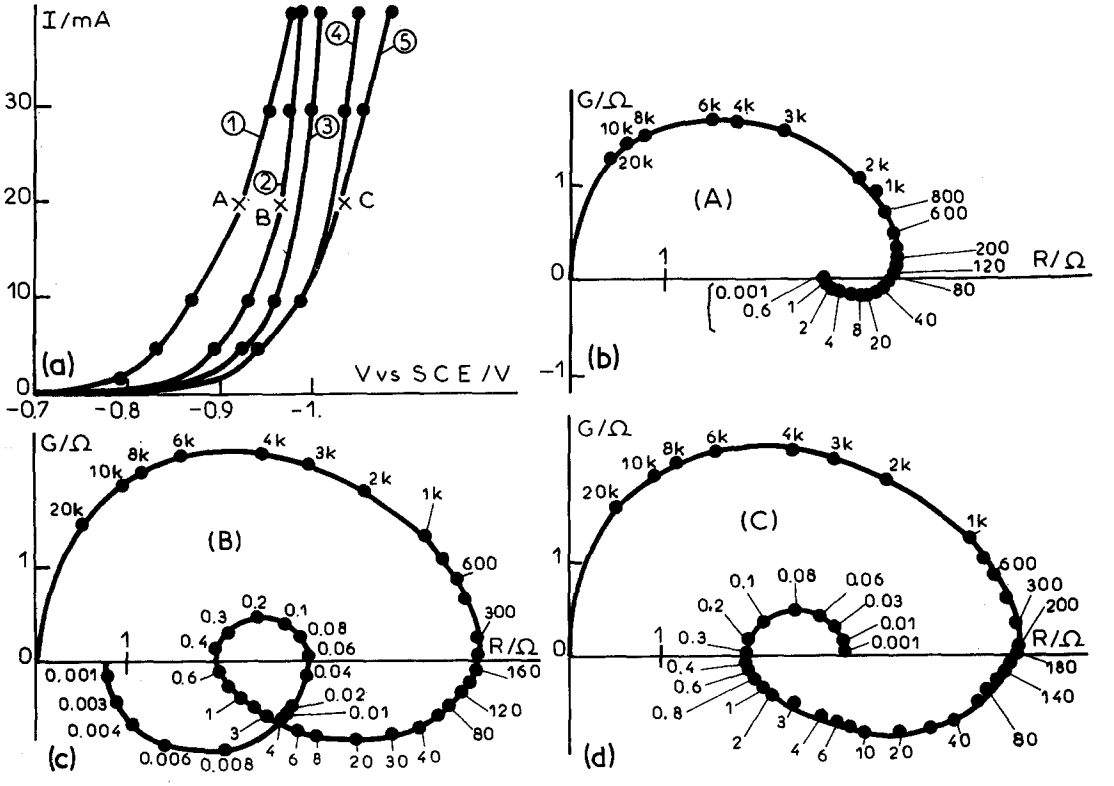

Fig. 1. (a) Steady-state current–potential curves plotted during nickel electrodeposition in Watts electrolyte (pH = 4·5; temperature 50° C). Rotating disc electrode (area 0·2 cm^2). Curve 1, Ω = 2000 rev min^{-1}; curve 2, Ω = 100 rev min^{-1}; curve 3, Ω = 200 rev min^{-1}; curve 4, Ω = 600 rev min^{-1}; curve 5, Ω = 2000 rev min^{-1}. Curve 1, no additives; curves 2–5, with 8 × 10^{-3} M B_2D_{14}. (b)–(d) Complex impedance ($Z = R - jG$) diagrams corresponding respectively to points A, B and C on curves 1, 2 and 5 (frequency in Hz).

rotation speed, it can be seen that the inhibiting effect diminishes with an increase of cathodic current.

This diffusion-controlled inhibition can be observed also on the impedance diagrams. As shown on Fig. 1c (obtained at point B on Fig. 1a) obtained at the same current as Fig. 1d, an additional inductive loop appears between 0·04 Hz and 0·001 Hz, without any neat change in the shape and characteristic frequencies of the rest of the diagram.

3.2. *Zinc electrocrystallization*

3.2.1. Influence of $PbAc_2$. The influence on the inhibiting effect of the additive has been investigated in both acid and alkaline media.

The results presented on Fig. 2 have been obtained with a Leclanché cell electrolyte whose $ZnCl_2$ concentration was 0·48 M. For the inhibitor-free electrolyte and with rotation speeds of the electrode higher than 1000 rev min^{-1}, the current–potential curve is vertical for a wide range of currents [9] as is depicted on Fig. 2a (curve 1). With 10^{-4} M $PbAc_2$ and under the same electrolysis conditions, the polarization curve is shifted towards more cathodic potentials (curve 5).

Fig. 2b (obtained at point D of Fig. 2a) and Fig. 2d (obtained at point F of Fig. 2a) are typical of impedance diagrams recorded without and with $PbAc_2$, respectively [2]. At frequencies lower than 200 Hz, it can be seen that the Faradaic impedance is modified by the additive. These modifications have already been interpreted in terms of specific changes in the rates of the interfacial reactions [3].

For lower rotation speeds Ω, a diffusion-controlled inhibition appears since current–potential curves become dependent on Ω: their

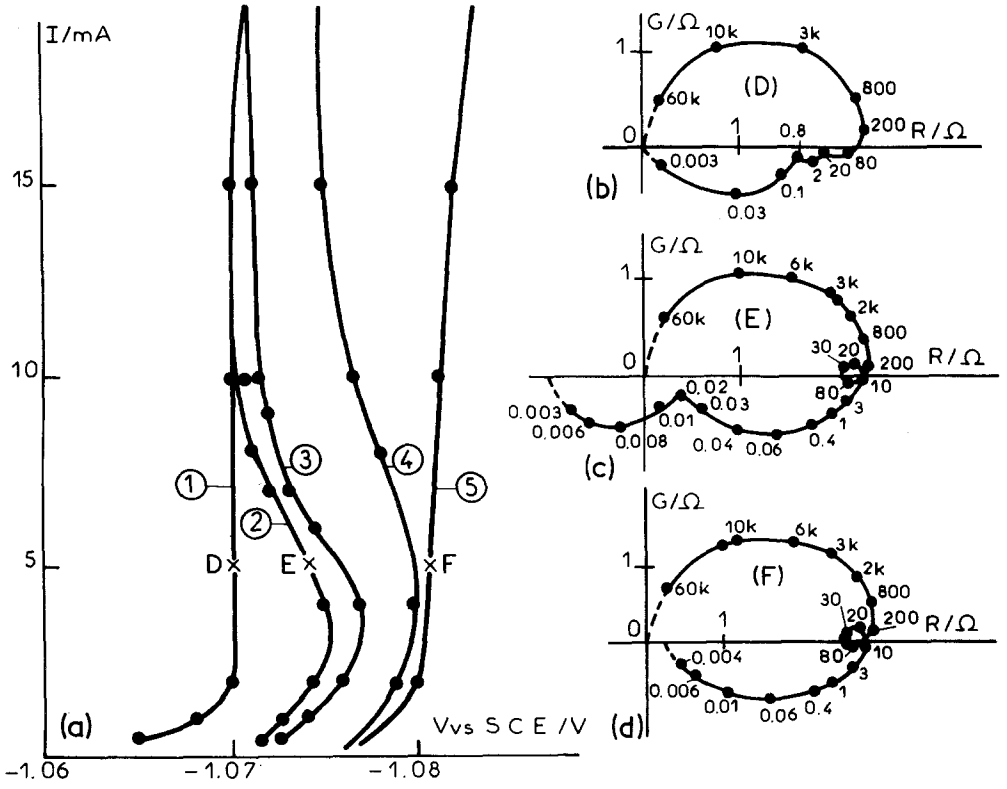

Fig. 2. (a) Steady-state current–potential curves plotted during zinc electrodeposition in the Leclanché cell electrolyte ($ZnCl_2$ 0·48 M). Rotating disc electrode (area 0·28 cm^2). Curve 1, Ω = 1000 rev min^{-1}; curve 2, Ω = 200 rev min^{-1}; curve 3, Ω = 400 rev min^{-1}; curve 4, Ω = 600 rev min^{-1}; curve 5, Ω = 1000 rev min^{-1}. Curve 1, no additives; curves 2–5, with 10^{-4} M $PbAc_2$. (b)–(d) Complex impedance ($Z = R - jG$) diagrams corresponding respectively to points D, E and F, on curves 1, 2 and 5 (frequency in Hz).

shift towards more negative potentials lessens when Ω decreases. In addition the inhibiting effect of $PbAc_2$ decreases with an increase of current thus producing S-shaped current–potential curves. Such multiple steady states originating from the diffusion-controlled inhibition of zinc electrodeposition appear clearly on curves 2, 3 and 4 in Fig. 2.

An additional inductive loop arises at low frequencies on impedance diagrams plotted for low rotation speeds. This is exemplified on Fig. 2c (obtained at point E on Fig. 2a) where this inductive loop appears under 0·02 Hz. It can be noticed that the extrapolation of this loop down to zero frequency leads to a negative polarization resistance corresponding to the negative slope of curve 2 at point E on Fig. 2a.

In the Leclanché cell electrolyte of higher $ZnCl_2$ concentration (0·72 M), a similar inhibiting effect of $PbAc_2$ has been observed as a function of rotation speed Ω, as seen on Fig. 3a. Since the multiple steady states have already appeared in the inhibitor-free electrolyte (curve 1), the consequence of a diffusion-controlled inhibition (curves 2, 3 and 4) is a widened range of current in which these multiple steady states occur. An elimination of the influence of mass transport gives a single-valued polarization curve (curve 5).

Fig. 3b (obtained at point G on Fig. 3a) corresponding to a diffusion-controlled inhibiting effect of $PbAc_2$ is similar to Fig. 2c.

Fig. 4a exhibits similar multiple steady states (curves 2 and 3) arising from the diffusion-controlled inhibition of zinc electrodeposition in the zincate alkaline electrolyte. On Fig. 4b (obtained at point H on Fig. 4a), the inductive loop due to the inhibitor diffusion still appears under 0·02 Hz.

3.2.2. Influence of NBu_4Br. The inhibiting effect of 5×10^{-5} M NBu_4Br is similar to that of $PbAc_2$ in both the Leclanché cell electrolyte (Fig. 5a looks like Fig. 3a) and the alkaline electrolyte (Fig. 6a looks like Fig. 4a). However it can be remarked that the shift of the current–potential curves is always far greater with NBu_4Br than with $PbAc_2$. This confirms previous results obained after eliminating the influence of mass transport [3, 10].

A comparison of impedance diagrams also reveals a systematic difference between the two additives: the frequency at the summit of the inductive loop for the lowest frequencies, which characterizes the slowest relaxation process, is close to 0·06 Hz for NBu_4Br on Figs. 5b (obtained at point I on Fig. 5a) and 6b (obtained at point J on Fig. 6a), instead of 0·008 Hz for $PbAc_2$ on Figs. 2c, 3b and 4b.

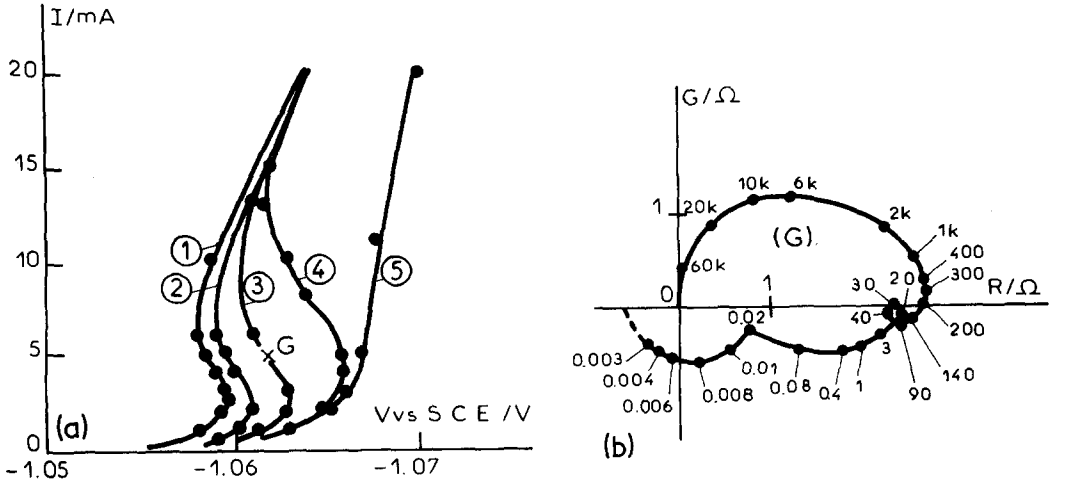

Fig. 3. (a) Steady-state current–potential curves plotted during zinc electrodeposition in the Leclanché cell electrolyte ($ZnCl_2$ 0·72 M). Rotating disc electrode (area 0·28 cm^2). Curve 1, Ω = 1000 rev min^{-1}; curve 2, Ω = 200 rev min^{-1}; curve 3, Ω = 300 rev min^{-1}; curve 4, Ω = 600 rev min^{-1}; curve 5, Ω = 1000 rev min^{-1}. Curve 1, no additives; curves 2–5, with 5×10^{-5} M $PbAc_2$. (b) Complex impedance ($Z = R - jG$) diagram corresponding to point G on curve 3 (frequency in Hz).

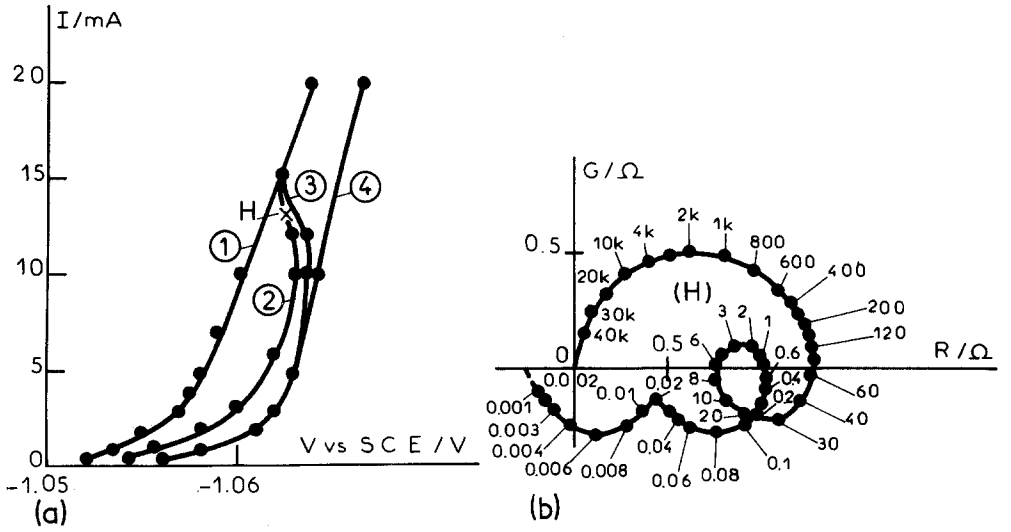

Fig. 4. (a) Steady-state current–potential curves plotted during zinc electrodeposition in the alkaline zincate electrolyte. Rotating disc electrode (area 0·28 cm^2). Curve 1, $\Omega = 1500$ rev min^{-1}; curve 2, $\Omega = 200$ rev min^{-1}; curve 3, $\Omega = 600$ rev min^{-1}; curve 4, $\Omega = 1500$ rev min^{-1}. Curve 1, no additives; curves 2–4, with 10^{-5} M $PbAc_2$. (b) Complex impedance ($Z = R - jG$) diagram corresponding to point H on curve 2 (frequency in Hz).

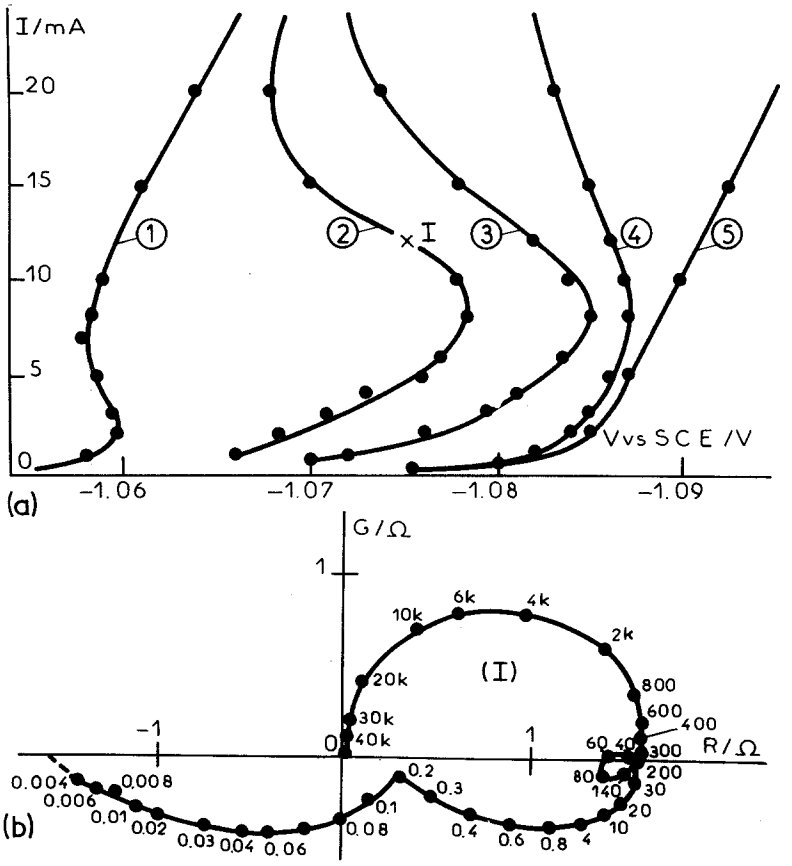

Fig. 5. (a) Steady-state current–potential curves plotted during zinc electrodeposition in the Leclanché cell electrolyte ($ZnCl_2$ 0·72 M). Rotating disc electrode (area 0·2 cm^2). Curve 1, $\Omega = 1000$ rev min^{-1}; curve 2, $\Omega = 100$ rev min^{-1}; curve 3, $\Omega = 200$ rev min^{-1}; curve 4, $\Omega = 500$ rev min^{-1}; curve 5, $\Omega = 1000$ rev min^{-1}. Curve 1, no additives; curves 2–5, with 5×10^{-5} M NBu_4Br. (b) Complex impedance ($Z = R - jG$) diagram corresponding to point I on curve 2 (frequency in Hz).

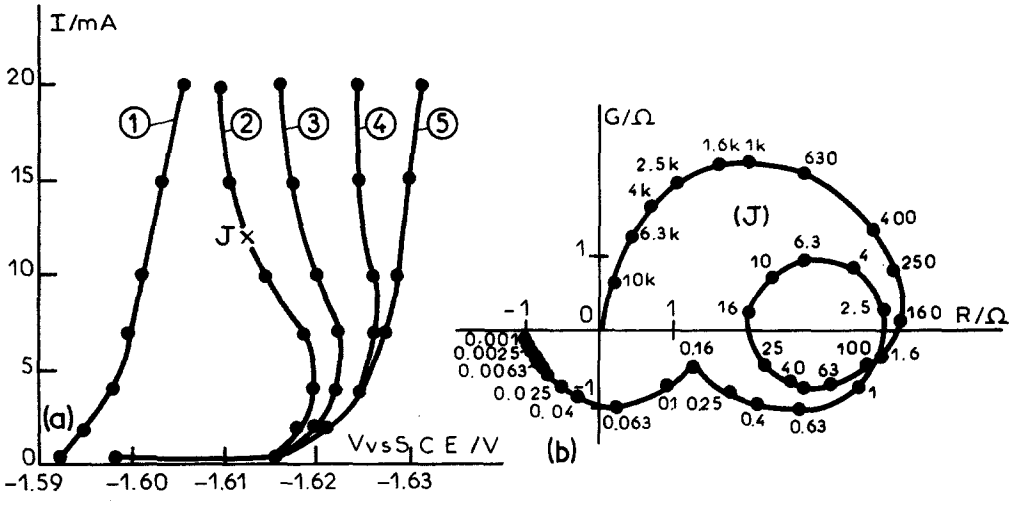

Fig. 6. (a) Steady-state current–potential curves plotted during zinc electrodeposition in the alkaline zincate electrolyte. Rotating disc electrode (area 0·2 cm^2). Curve 1, $\Omega = 1500$ rev min^{-1}; curve 2, $\Omega = 100$ rev min^{-1}; curve 3, $\Omega = 200$ rev min^{-1}; curve 4, $\Omega = 500$ rev min^{-1}; curve 5, $\Omega = 1500$ rev min^{-1}. Curve 1, no additives; curves 2–5, with 5×10^{-5} M NBu_4Br. (b) Complex impedance ($Z = R - jG$) diagram corresponding to point J on curve 2 (frequency in Hz).

3.3. *On the significance of the slowest relaxation process*

The above results reveal that the impedance diagrams plotted under conditions of diffusion-controlled inhibition always exhibit an additional inductive loop for low frequencies. The frequency characteristic of this slowest relaxation process varies with the kind of additives as observed in the case of zinc deposition.

These results raise a question: does this loop at low frequencies originate only from the diffusion of inhibitors towards the cathode? In such a case, the diffusion coefficient of inhibitors could be deduced from the diffusion loop since a diffusion impedance Z_d is given [11, 12] to a first approximation, by the relationship

$$Z_d = R_d \frac{\text{th}\sqrt{j2\pi f\delta^2/D}}{\sqrt{j2\pi f\delta^2/D}} \qquad (1)$$

where R_d is a diffusion resistance, $j = \sqrt{-1}$, f the frequency, δ the thickness of the Nernst diffusion layer, and D the diffusion coefficient of transported species.

For a rotating disc electrode

$$\delta = 1{\cdot}61\, D^{1/3}\nu^{1/6}\Omega^{-1/2} \qquad (2)$$

where ν is the kinematic viscosity of the electrolyte. The frequency f_m at the summit of the diffusion loop is given by [12]

$$2\pi f_m\delta^2/D = 2{\cdot}53 \qquad (3)$$

and allows a determination of D.

The application of Equation 3 to our impedance measurements, taking $\nu = 10^{-2}\,cm^2\,s^{-1}$, leads to values of D given in Table 1.

The calculated data do not correspond to reasonable values for the diffusion coefficient D, whose order of magnitude would rather be close to 10^{-5} cm^2 s^{-1}. This means that the loop at lowest frequencies is not merely governed by the inhibitor diffusion, but probably also results from an interfacial process (possibly the adsorption–desorption of inhibitors) slower than this diffusion.

It has to be noted that the coupled processes which give rise to the slowest relaxation are closely connected with the interfacial reactions leading to the metal deposit. Particularly for zinc deposition, a comparison of the various impedance diagrams obtained with the two inhibitors shows that the relaxation frequency, in the loop at lowest frequencies, varies with that of the nearest inductive loop which expresses the relaxation of the surface concentration of kink sites [13]. In the presence of NBu_4Br it has already been shown that the production and removal of kink sites are much more accelerated than with $PbAc_2$ [3]. The

Table 1. Calculated values of D *according to Equation 3*

Inhibitor	*Impedance diagram*	f_m (Hz)	Ω (rev min^{-1})	D ($cm^2\ s^{-1}$)
B_2D_{14}	Fig. 1c	0·008	100	10^{-9}
$PbAc_2$	Fig. 3b	0·008	300	5×10^{-11}
NBu_4Br	Fig. 5b or 6b	0·06	100	5×10^{-9}

present results are in agreement and indicate that the characteristic frequency of the loop at lowest frequencies is higher with NBu_4Br than with $PbAc_2$. Thus at least for zinc electrodeposition, the loop at lowest frequencies seems to be the consequence of a coupling between the diffusion of inhibitors, their adsorption and certain interfacial reactions leading to zinc deposits.

4. Conclusion

Investigated with a rotating disc electrode the diffusion-controlled inhibition of zinc electrodeposition is able to give rise to, or to emphasize the existence of, multiple steady states observed on current–potential curves which depend on the electrode rotation speed.

For both nickel and zinc electrodeposition such a diffusion-controlled influence of additives appears also on impedance measurements revealing an additional inductive loop at low frequencies. The time constant indicates that this inductive loop does not result only from the inhibitor diffusion but also from interfacial processes slower than diffusion. At least for zinc deposition, it appears that these interfacial processes involve the slow formation and removal of growth kink sites at the electrode surface.

References

[1] I. Epelboin and R. Wiart, *J. Electrochem. Soc.* **118** (1971) 1577.
[2] J. Bressan and R. Wiart, *J. Appl. Electrochem.* 7 (1977) 505.
[3] *Idem, ibid* 9 (1979) 43.
[4] O. Kardos, *Plating* **61** (1974) 129, 229, 316.
[5] R. Wiart, *Oberfläche-Surface* 9 (1968) 213, 241, 275.
[6] Ph. Morel, *Trait. Surface* 89 (1969) 9.
[7] *Idem, ibid* **91** (1970) 355.
[8] C. Gabrielli, M. Ksouri and R. Wiart, *Electrochim. Acta* 22 (1977) 255.
[9] I. Epelboin, M. Ksouri, E. Lejay and R. Wiart, *Electrochim. Acta* **20** (1975) 603.
[10] J. Bressan, M. Ksouri and R. Wiart, *28th Meeting ISE*, Druzhba (1977), Extended Abstracts, 'Electrocrystallization' p. 34.
[11] D. Schuhmann, *Compt. Rend.* **262** (1966) 1125.
[12] C. Deslouis, I. Epelboin, M. Keddam and J. C. Lestrade, *J. Electroanalyt. Chem.* 28 (1970) 57.
[13] I. Epelboin, M. Ksouri and R. Wiart, *12th Faraday Disc. Chem. Soc.* Southampton (1978) p. 115.